Unified edge-oriented stabilization of nonconforming finite element methods for incompressible flow problems

Abderrahim Ouazzi and Stefan Turek

Institute of Applied Mathematics, University of Dortmund, 44227 Dortmund, Germany
Abderrahim.Ouazzi@math.uni-dortmund.de, *Stefan.Turek@math.uni-dortmund.de*

Summary. This paper deals with various aspects of edge-oriented stabilization techniques for nonconforming finite element methods for the numerical solution of incompressible flow problems. We discuss two separate classes of problems which require appropriate stabilization techniques: First, the lack of coercivity for nonconforming low order approximations for treating problems with the symmetric deformation tensor instead of the gradient formulation in the momentum equation ('Korn's inequality') which particularly leads to convergence problems of the iterative solvers for small Reynolds (Re) numbers. Second, numerical instabilities for high Re numbers or whenever convective operators are dominant such that the standard Galerkin formulation fails and leads to spurious oscillations. We show that the right choice of edge-oriented stabilization is able to provide simultanously excellent results regarding robustness and accuracy for both seemingly different cases of problems, and we discuss the sensitivity of the involved parameters w.r.t. mesh distortions and variations of the Re number. Moreover, we explain how efficient multigrid solvers can be constructed to circumvent the problems with the arising 'non-standard' FEM data structures, and we provide several examples for the numerical efficiency for realistic flow configurations with benchmarking character.

1 Introduction

Stabilization techniques for (nonconforming) FEM discretizations in the context of incompressible flow problems, for instance described by the Navier-Stokes equations or appropriate extensions in multiphase problem settings, are still a challenging task. In this paper, particularly from a practical point of view, we want to analyze special edge-oriented stabilization approaches regarding the following three aspects:

I. Necessity. There are two well-known situations for nonconforming finite element methods when severe numerical problems may arise: the lack of coercivity for nonconforming low order approximations for symmetric deformation tensor formulations, mainly visible for the iterative solvers for small Re numbers, and whenever convective operators are dominant, for instance for medium and high Re numbers or for the treatment of pure transport problems. Then, the standard Galerkin formulation fails and may lead to numerical oscillations and convergence problems of the iterative solvers, too.

II. Robustness. To analyze the quality of edge-oriented stabilization terms for a wide range of Re numbers and for different problem types is one of the central tasks for the use of edge-oriented stabilization techniques as black box tools in future CFD codes. Here, the question of appropriate parameter settings and stabilization terms is always a delicate task, particularly on general meshes.

II. Efficiency. One disadvantage of edge-oriented stabilization is the contribution of an additional layer of neighboring elements via jumps across the edges of the computational mesh. So, a new sparsity pattern

for the resulting stiffness matrix is introduced which may contradict to the usual data structures of finite element methods. In the context of preconditoned Krylov-space or multigrid solvers, we show how suitable preconditioners in the framework of defect-correction schemes can be applied.

Our contribution has the goal to critically discuss these 3 aspects via numerical analysis which we restrict to the incompressible Navier-Stokes equations since they contain already most of the typical difficulties. Extensions to more complex problems, for instance multiphase or visco-elastic flow, are possible and are described, for instance, in [18].

1.1 Problem formulation

As a model problem we consider incompressible flow problems described by the generalized Navier-Stokes equations. The Cauchy stress tensor is given by $\sigma = 2\nu(D_{II}(\boldsymbol{u}), p)\mathbf{D}(\boldsymbol{u}) - p\mathbf{I}$, where p is the pressure; $\mathbf{D}(\boldsymbol{u}) = \frac{1}{2}(\nabla\boldsymbol{u} + \nabla^T\boldsymbol{u})$ is the rate of the deformation tensor, $\boldsymbol{u}$ denotes the velocity; $\nu(\cdot)$ is the (nonlinear) viscosity which may depend on the second invariant of the rate deformation tensor $D_{II}(\boldsymbol{u}) = \frac{1}{2}\,\mathrm{tr}(\mathbf{D}^2(\boldsymbol{u}))$ and the pressure p. Then, depending on the specific viscosity function $\nu(\cdot)$ we consider the following prototypical models (with appropriate parameters ν_0, r):

- Newtonian flow defined for $\nu(z,p) = \nu_0$

In this case of a newtonian fluid with constant viscosity, we replace the deformation tensor $\mathbf{D}(\boldsymbol{u})$ by the usual formulation with the gradient $\nabla\boldsymbol{u}$ only.

- Non-newtonian flow due to *Power law*, with $\nu(z,p) = \nu_o z^{\frac{r}{2}-1}$, resp., *Bingham law* with $\nu(z,p) = \nu_o z^{-\frac{1}{2}}$
- Non-newtonian flow with pressure and shear-dependent viscosity, as described for instance in [10, 17] or in the case of the *Schaeffer model* [20], with $\nu(z,p) = \nu_0 p z^{-\frac{1}{2}}$, for granular powder flow

In all cases, the velocity $\boldsymbol{u}$ and the pressure p satisfy the following generalized Navier-Stokes equations

$$\frac{\partial \boldsymbol{u}}{\partial t} + \boldsymbol{u}\cdot\nabla\boldsymbol{u} - \mathrm{div}\,(2\nu(D_{II}(\boldsymbol{u}),p)\mathbf{D}(\boldsymbol{u})) + \nabla p = \boldsymbol{f}, \quad \mathrm{div}\,\boldsymbol{u} = 0\,, \tag{1}$$

resp., for newtonian flow with constant viscosity

$$\frac{\partial \boldsymbol{u}}{\partial t} + \boldsymbol{u}\cdot\nabla\boldsymbol{u} - \nu\Delta\boldsymbol{u} + \nabla p = \boldsymbol{f}, \quad \mathrm{div}\,\boldsymbol{u} = 0\,. \tag{2}$$

In the following, we mainly consider the stationary generalized Navier-Stokes problem (1) in a bounded domain $\Omega \subset \mathbb{R}^2$, and we use the rate of the deformation tensor instead of the gradient formulation as in (2), unless it is stated explicitely. If we restrict the set V of test functions to be divergence-free and if we take the constitutive laws into account, the above (stationary) equations (1) lead to:

$$\int_\Omega 2\nu(D_{II}(\boldsymbol{u}),p)\mathbf{D}(\boldsymbol{u}) : \mathbf{D}(\boldsymbol{v})\,dx + \int_\Omega (\boldsymbol{u}\cdot\nabla\boldsymbol{u})\boldsymbol{v}\,dx = \int_\Omega \boldsymbol{f}\boldsymbol{v}\,dx,\ \forall \boldsymbol{v} \in V \tag{3}$$

It is straightforward to penalize the constraint $\operatorname{div} \boldsymbol{v} = 0$ to derive the equivalent mixed formulations:

Find $(\boldsymbol{u}, p) \in X \times M$ *such that*

$$\begin{aligned} \int_\Omega 2\nu(D_{\mathrm{II}}(\boldsymbol{u}), p)\mathbf{D}(\boldsymbol{u}) : \mathbf{D}(\boldsymbol{v})\, dx + \int_\Omega (\boldsymbol{u}\cdot\nabla\boldsymbol{u})\boldsymbol{v}\, dx \quad &+ \int_\Omega p \operatorname{div}\boldsymbol{v}\, dx \\ = \int_\Omega \boldsymbol{f}\boldsymbol{v}\, dx, \qquad &\forall \boldsymbol{v} \in X, \\ \int_\Omega q \operatorname{div}\boldsymbol{u}\, dx = 0, \qquad &\forall q \in M, \end{aligned} \tag{4}$$

with the spaces $X = [H_0^1(\Omega)]^2$ and $M = L^2(\Omega)$. In some test calculations, we also consider related Stokes problems, which means that we omit the convective term $\int_\Omega (\boldsymbol{u}\cdot\nabla\boldsymbol{u})\boldsymbol{v}\, dx$. For the following analysis, we introduce the bilinear forms:

$$\langle \mathbf{A}(\boldsymbol{w}, q)\boldsymbol{u}, \boldsymbol{v}\rangle = \int_\Omega 2\nu(D_{\mathrm{II}}(\boldsymbol{w}), q)\mathbf{D}(\boldsymbol{u}) : \mathbf{D}(\boldsymbol{v})\, dx \tag{5}$$

$$\langle \mathbf{N}(\boldsymbol{w})\boldsymbol{u}, \boldsymbol{v}\rangle = \int_\Omega (\boldsymbol{w}\cdot\nabla\boldsymbol{u})\boldsymbol{v}\, dx \quad , \quad \langle \mathbf{B}q, \boldsymbol{v}\rangle = \int_\Omega q \operatorname{div}\boldsymbol{v}\, dx \tag{6}$$

Then, we can rewrite our generalized flow problems in the following compact form:

Find $(\boldsymbol{u}, p) \in X \times M$ *such that*

$$\begin{aligned} \langle \mathbf{A}(\boldsymbol{u}, p)\boldsymbol{u}, \boldsymbol{v}\rangle + \langle \mathbf{N}(\boldsymbol{u})\boldsymbol{u}, \boldsymbol{v}\rangle + \langle \mathbf{B}p, \boldsymbol{v}\rangle = \int_\Omega \boldsymbol{f}\boldsymbol{v} dx, \quad &\forall \boldsymbol{v} \in X, \\ \langle \mathbf{B}q, \boldsymbol{u}\rangle = 0, \qquad &\forall q \in M. \end{aligned} \tag{7}$$

1.2 Nonconforming finite element discretization

We consider a subdivision $T \in \mathcal{T}_h$ consisting of quadrilaterals in the domain $\Omega_h \in \mathbb{R}^2$, and we employ the nonconforming rotated bilinear *Rannacher-Turek* element [19]. For any quadrilateral T, let (ξ, η) denote a local coordinate system obtained by joining the midpoints of the opposing faces of T. Then, in the *nonparametric* case, we set on each element T

$$\tilde{Q}_1(T) := span\left\{1, \xi, \eta, \xi^2 - \eta^2\right\}. \tag{8}$$

The degrees of freedom are determined by the nodal functionals $\{F_\Gamma^{(a,b)}(\cdot), \Gamma \subset \partial\mathcal{T}_h\}$,

$$F_\Gamma^a := |\Gamma|^{-1} \int_\Gamma v d\gamma \quad \text{or} \quad F_\Gamma^b := v(m_\Gamma) \quad (m_\Gamma \text{ midpoint of edge } \Gamma) \tag{9}$$

such that the finite element space can be written as

$$\begin{aligned} W_h^{a,b} := \{v \in L_2(\Omega_h), v \in \tilde{Q}_1(T), \forall T \in \mathcal{T}_h, v \text{ continuous w.r.t. all} \\ \text{nodal functionals } F_{\Gamma_{i,j}}^{a,b}(\cdot), \text{ and } F_{\Gamma_{i0}}^{a,b}(v) = 0, \forall \Gamma_{i0}\}. \end{aligned} \tag{10}$$

Here, $\Gamma_{i,j}$ denote all inner edges sharing the two elements i and j, while Γ_{i0} denote the boundary edges of $\partial\Omega_h$. In this paper, we always employ version 'a' with the integral mean values as degrees of freedom. Then, the corresponding discrete functions will be approximated in the spaces

$$V_h := W_h^a \times W_h^a \,,\; L_h := \left\{ q_h \in L^2(\Omega), q_{h|\mathcal{T}} = \text{const.}, \forall \mathcal{T} \in \mathcal{T}_h \right\}. \tag{11}$$

Due to the loss of global continuity of the discrete velocities, the classical (discrete) 'Korn's Inequality', $\sum_{\mathcal{T}\in\mathcal{T}_h} \|\boldsymbol{v}\|_{H^1(\mathcal{T})} \leq c\,(\sum_{\mathcal{T}\in\mathcal{T}_h} \|\boldsymbol{v}\|^2_{L^2(\mathcal{T})} + \|\mathbf{D}(\boldsymbol{v})\|^2_{L^2(\mathcal{T})})^{\frac{1}{2}}$, is not satisfied which is important for problems involving the symmetric part $\mathbf{D}(\boldsymbol{u})$ of the gradient [14]. Therefore, appropriate edge-oriented stabilization techniques (see [1, 9, 22]) have been proposed which directly incorporate the jump across the inter-elementary boundaries. Another source of problems for FEM discretizations, not only for nonconforming finite elements, is the case of dominant convection, that means the case of medium and high Re numbers or if additional tracer equations are included. Consequently, in the following sections we discuss several stabilizations techniques for both sources of instability.

2 Short review on stabilization techniques for nonconforming finite element methods for incompressible flow

This section is provided to present a short overview on (typical) stabilization techniques for nonconforming FEM in the case of dominating convection and for satisfying Korn's inequality.

2.1 Classical stabilization methods

FEM upwinding

The main idea is to introduce new edge-centered lumping regions and special lumping operators (for details see [21]). Then, the discrete convective operator $\langle \mathbf{N}(\boldsymbol{u}_h)\boldsymbol{v}_h, \boldsymbol{w}_h\rangle$ is replaced by

$$\langle \tilde{\mathbf{N}}(\boldsymbol{u}_h)\boldsymbol{v}_h, \boldsymbol{w}_h\rangle = \sum_l \sum_{k\in\Lambda_l} \oint_{\Gamma_{lk}} \boldsymbol{u}_h \cdot \boldsymbol{n}_{lk} d\gamma [1 - \lambda_{lk}(\boldsymbol{u}_h)(\boldsymbol{v}_h(m_k) - \boldsymbol{v}_h(m_l))]\boldsymbol{w}_h(m_l). \tag{12}$$

Based on the local Reynolds number Re_T on each cell T (see [21] for details)

$$Re_T = \frac{\|\boldsymbol{u}\|_{\infty,T} \cdot h_T}{\nu} \tag{13}$$

we can define:

$$\lambda_{lk}(u_h) = \begin{cases} \dfrac{\frac{1}{2} + \delta^* Re_T}{1 + \delta^* Re_T} & \text{if } Re_T \geq 0 \\ \dfrac{1}{2(1 - \delta^* Re_T)} & \text{otherwise} \end{cases} \tag{14}$$

Here, h_T is a local mesh size parameter on each cell T which can be critical on highly distorted meshes. Moreover, the appropriate choice of the free parameter δ^* is quite sensitive and can significantly influence the resulting accuracy as the following test calculations will demonstrate.

FEM streamline-diffusion

This method was originally proposed by, for instance, Johnson [13] and by Hughes and Brooks [11], and it has been successfully applied to several classes of problems since streamline-diffusion methods can combine good stability and high accuracy. So, due to its simplicity, streamline-diffusion is a common tool used in many (commercial) CFD codes. It mainly consists of adding the following stabilization term to the original convection operator described by $\langle \mathbf{N}(\boldsymbol{u}_h)\boldsymbol{v}_h, \boldsymbol{w}_h\rangle$, that means:

$$\langle \tilde{\mathbf{N}}(\boldsymbol{u}_h)\boldsymbol{v}_h, \boldsymbol{w}_h\rangle = \langle \mathbf{N}(\boldsymbol{u}_h)\boldsymbol{v}_h, \boldsymbol{w}_h\rangle + \sum_{T\in T_h} \delta_T \int_T (\boldsymbol{u}_h \cdot \nabla \boldsymbol{v}_h)(\boldsymbol{u}_h \cdot \nabla \boldsymbol{w}_h) dx \tag{15}$$

Here, the critical quantity for an efficient computational treatment is the local damping parameter δ_T. A usual setting is described, for instance, in [21]. The local Reynolds number Re_T can be introduced as before and we can define, for instance,

$$\delta_T = \delta^* \cdot \frac{h_T}{\|\boldsymbol{u}\|_{\infty,\Omega}} \cdot \frac{2Re_T}{1+Re_T}. \tag{16}$$

Due to the more complex bilinear form, including numerical integration in certain quadrature points, the numerical work for the matrix assembling process is increased and, again, the precise definition of δ^* and h_T, particularly on strongly anisotropic meshes containing large aspect ratios, can be critical. And, finally, the application to nonsteady problems and the extension to more complex coupled problems or systems, as for instance Boussinesq approximations or multiphase flow problems is not fully clear.

2.2 Edge-oriented stabilization methods

The main idea is to augment the original finite element discretization by an interior penalty term involving the jump of the function values or of the gradient of the approximate FEM solution. The jump for a function $\boldsymbol{u}$ on an edge from ∂T can be defined by

$$[\boldsymbol{u}] = \begin{cases} \boldsymbol{u}^+ \cdot \boldsymbol{n}^+ + \boldsymbol{u}^- \cdot \boldsymbol{n}^- & \text{on internal edges,} \\ \boldsymbol{u} \cdot \boldsymbol{n} & \text{on Dirichlet boundary edges,} \\ 0 & \text{on Neumann boundary edges,} \end{cases} \tag{17}$$

where $\boldsymbol{n}$ is the outward normal to the edge and $(\cdot)^+$ and $(\cdot)^-$ indicate the value of the generic quantity $(\cdot)$ on the two elements sharing the same edge. In the literature, several jump terms were introduced for different situations:

I. Jump terms including function values

$$j_1(\boldsymbol{u}, \boldsymbol{v}) = \sum_{\text{edge E}} \gamma\nu \frac{1}{|E|} \int_E [\boldsymbol{u}][\boldsymbol{v}] d\sigma \tag{18}$$

John et al. [12] introduced the jump term in the nonconforming streamline-diffusion method for convection dominated problem to achieve the same accuracy as with conforming streamline-diffusion FEM methods. Moreover, to satisfy the discrete Korn's inequality, variants have been presented by Hansbo and Larson in [9] and by Turek, Ouazzi and Schmachtel in [22]. And, in a similar way, an analogous approach for a general Korn's inequality for piecewise H^1-functions has been introduced by Brenner in [1].

II. Jump terms including the gradient

$$
\begin{aligned}
j_{2,\alpha}(\boldsymbol{u},\boldsymbol{v}) &= \sum_{\text{edge E}} \gamma |E|^{\alpha} \int_E [\nabla \boldsymbol{u}][\nabla \boldsymbol{v}] d\sigma \\
j_{3,\alpha}(\boldsymbol{u},\boldsymbol{v}) &= \sum_{\text{edge E}} \gamma |E|^{\alpha} \int_E [\boldsymbol{n}\cdot\nabla \boldsymbol{u}][\boldsymbol{n}\cdot\nabla \boldsymbol{v}] d\sigma \\
j_{4,\alpha}(\boldsymbol{u},\boldsymbol{v}) &= \sum_{\text{edge E}} \gamma |E|^{\alpha} \int_E [\boldsymbol{t}\cdot\nabla \boldsymbol{u}][\boldsymbol{t}\cdot\nabla \boldsymbol{v}] d\sigma \\
j_{5,\alpha}(\boldsymbol{u},\boldsymbol{v}) &= \sum_{\text{edge E}} \gamma |E|^{\alpha} \int_E [(\boldsymbol{t}\cdot\nabla \boldsymbol{u})\cdot\boldsymbol{n}][(\boldsymbol{t}\cdot\nabla \boldsymbol{v})\cdot\boldsymbol{n}] d\sigma
\end{aligned}
\tag{19}
$$

These terms (with different values for α) for stabilizing convection dominated problems have been introduced by Burman, Hansbo et al. in [6, 7], see also [3] and [5].

III. Jump terms including the divergence

$$
j(\boldsymbol{u},\boldsymbol{v}) = \sum_{\text{edge E}} \gamma |E|^{2} \int_E [\nabla\cdot \boldsymbol{u}][\nabla\cdot \boldsymbol{v}] d\sigma \tag{20}
$$

This approach was originally proposed by Burman, Hansbo et al. in [7] to control the incompressibility condition.

IV. Jump terms including the normal component of function values

$$
j(\boldsymbol{u},\boldsymbol{v}) = \sum_{\text{edge E}} \gamma \nu \frac{1}{|E|} \int_E [\boldsymbol{n}\cdot \boldsymbol{u}][\boldsymbol{n}\cdot \boldsymbol{v}] d\sigma \tag{21}
$$

To control the nonconformity arising from the pressure term in Darcy's law, this term has been introduced by Burman and Hansbo in [4].

The terms proposed in III. and IV. will not be discussed in the following since they are not essential for the stabilization of Korn's inequality, resp., of convection dominated flow which is the main aim of our studies in this paper. So, summarizing this overview, it shows that for different types of problems corresponding jump terms with "free" constant γ and order $|E|^{\alpha}$ have been introduced. Our aim in this contribution is to analyze a new variant which uses only one jump term and one choice for the free parameter γ, and which is nevertheless able to simultanously treat both types of problems. To be precise, we propose the following jump term, resp., discrete stabilization term (with $h_E = |E|$)

$$
\langle \mathbf{S}\boldsymbol{u}_h, \boldsymbol{v}_h\rangle = \sum_{\text{edge E}} \max(\gamma^* \nu h_E, \gamma h_E^2) \int_E [\nabla \boldsymbol{u}_h][\nabla \boldsymbol{v}_h] d\sigma \tag{22}
$$

which will be added to the original bilinear form, resp., discretized stiffness matrices, and which uses only the gradient of the approximate solution. This approach is based on a blending of (18), applying an appropriate scaling with h_E^2 due to the gradient of the discrete trial, resp., test functions, together with the formula in (19), applying $\alpha = 2$. In the case of nonlinear viscosity ν, this stabilization term may depend in a nonlinear way on the solution, too. The parameters γ, γ^* can be chosen - more or less arbitrarily as the subsequent tests will show - in the interval $[0.0001, 0.1]$, with no significant influence on the resulting accuracy, robustness and efficiency.

Summarizing, we can differ between the following situations:

1. In the case of treating the convective operators, $\boldsymbol{u}\cdot\nabla\boldsymbol{u}$, the upwinding and the streamline-diffusion approach modify the original discrete convective operator $\langle \mathbf{N}(\boldsymbol{u}_h)\boldsymbol{v}_h, \boldsymbol{w}_h\rangle$ by an operator $\langle \tilde{\mathbf{N}}(\boldsymbol{u}_h)\boldsymbol{v}_h, \boldsymbol{w}_h\rangle$ which may depend in a nonlinear way on the solution $\boldsymbol{u}_h$ itself via the local Re number; in contrast, the edge-oriented technique always adds a linear operator $\langle \mathbf{S}\boldsymbol{u}_h, \boldsymbol{v}_h\rangle$, unless an additional (nonlinear) shock-capturing term is used.
2. In the case of treating the deformation tensor formulation, $\mathbf{D}(\boldsymbol{u})$, the edge-oriented approach employs an additional stabilization term which mainly depends on the size of the viscosity ν; if ν depends on the solutions $\boldsymbol{u}_h$ and p_h, then this stabilization can become nonlinear. In the case of upwinding and streamline-diffusion, a corresponding stabilization is only performed if the convective operator is getting dominant. That means that for very low Re numbers, but with deformation tensor, no stabilization is applied since the local Re number vanishes.

3 Nonlinear and linear solvers

For treating the arising nonlinearities due to the described convective operator $\boldsymbol{u}\cdot\nabla\boldsymbol{u}$, resp., due to the nonlinear viscosity function ν, we apply standard quasi-Newton techniques of defect-correction type (see [15, 21]). Then, in every nonlinear iteration, the residuals of the discretized momentum and continuity equation involving the last iterate are calculated, while auxiliary linear saddle-point problems, mainly generalized Oseen equations, have to be solved in every step.

3.1 Sparsity of the matrix

Sparse matrices are an integral part of the finite element analysis for incompressible flow problems which may lead to huge and ill-conditioned systems for such Oseen-type problems so that very fast solvers of Krylov-space or particularly of multigrid type are required. However, the introduced edge-oriented stabilization techniques destroy the typical local sparsity properties since this approach involves more than the adjacent elements as can be seen in Figure 1 which shows the increased local support of nonconforming basis functions: The corresponding rows and columns for the new stiffness matrices $\mathbf{S}$ may contain 23 non-zero matrix elements, in contrast to the usual 7 for the non-stabilized case in 2D.

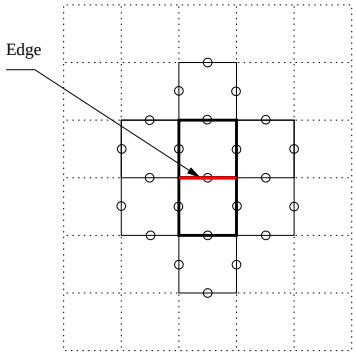

Fig. 1. Involved edges for each nonconforming basis function

To overcome the problem of storing the new matrix $\mathbf{S}$ - coming from $\langle \mathbf{S}\boldsymbol{u}_h, \boldsymbol{v}_h \rangle$ - with regard to the standard FEM data structures, we write the matrix $\mathbf{S}$ as a sum of two matrices $\mathbf{S}^*$ and $\mathbf{S}_{rest}$,

$$\mathbf{S} = \mathbf{S}^* + \mathbf{S}_{rest} \tag{23}$$

where $\mathbf{S}^*$ has the same sparsity structure as the usual corresponding finite element matrix; then, $\mathbf{S}_{rest} = \mathbf{S} - \mathbf{S}^*$. Hence, $\mathbf{S}^*$ can be handled with the same linear algebra techniques which are typically used for the treatment of the standard nonconforming finite element approach; $\mathbf{S}_{rest}$ is the complementary part and will be used as a correction for the calculation of the residuals inside of the linear solvers only. Then, given any approximation $\boldsymbol{v}$ and $\mathbf{A}$ denoting the (partial) stiffness matrix <u>without</u> the new stabilization matrices, we can write the complete residual as:

$$\boldsymbol{f} - (\mathbf{A} + \mathbf{S})\boldsymbol{v} = \boldsymbol{f} - (\mathbf{A} + \mathbf{S}^*)\boldsymbol{v} - \mathbf{S}_{rest}\boldsymbol{v} \tag{24}$$

Consequently, we store in the stiffness matrix only the partial matrix $\mathbf{A} + \mathbf{S}^*$ so that the first part of the residual can be obtained via standard matrix-vector multiplication while the second part of the residual is assembled via elementwise operations only. Moreover, the construction of preconditioners for the corresponding linear systems may only include parts of the (sub)matrix $\mathbf{A} + \mathbf{S}^*$, too, which will be explained in the following (see also [22] for more details).

3.2 Pressure Schur complement smoothers as defect-correction schemes

'Local Pressure Schur complement' schemes (see [15, 21]) as generalization of so-called 'Vanka smoothers' [25] are simple iterative relaxation methods for such coupled systems of saddle-point type which are acting directly on element level and which are embedded into an outer block Jacobi/Gauss-Seidel iteration. The local character of this procedure together with a global defect-correction mechanism is crucial for our approach. If we denote by $\mathbf{Res}_u$ and $\mathbf{Res}_p$ the residuals for the (complete) discrete momentum and continuity equations which include the complete stabilization term due to $\mathbf{S}$ as described in (24), one basic iteration step - that is one smoothing step - can be described as:

$$\begin{bmatrix} \boldsymbol{u}^{n+1} \\ p^{n+1} \end{bmatrix} = \begin{bmatrix} \boldsymbol{u}^{n} \\ p^{n} \end{bmatrix} + \omega^n \sum_i \begin{pmatrix} \mathbf{A}_{|\Omega_i} + \mathbf{S}^*_{|\Omega_i} & \mathbf{B}_{|\Omega_i} \\ \mathbf{B}^T_{|\Omega_i} & 0 \end{pmatrix}^{-1} \begin{bmatrix} \mathbf{Res}_u(u^n, p^n) \\ \mathbf{Res}_p(u^n, p^n) \end{bmatrix} \tag{25}$$

In our case, the *patches* Ω_i may consist of only one element which means that we restrict the global stiffness matrix to the single cells/quadrilaterals of the mesh and solve the corresponding algebraic problem. As can be seen, for the preconditioning step only parts of the matrix (here: $\mathbf{A}+\mathbf{S}^*$) are involved while the residual contains <u>all</u> parts of the matrix. Consequently, when this approach converges, the result is the solution of the stabilized version while the preconditioning steps only determine the speed of the overall iteration procedure. All other components in the multigrid approach, that means intergrid transfer, coarse grid correction and coarse grid solver, are the standard ones and are based on the underlying mesh hierarchy and the properties of the nonconforming finite elements (see [21] and [22] for the details).

4 Numerical Examples

In the subsequent sections, we will analyze the numerical behaviour of edge-oriented stabilization techniques, particularly of our proposed choice in (22), in comparison to upwinding and streamline-diffusion approaches, hereby regarding the following aspects:

- problems with medium and high Reynolds number
- problems with discrete Korn's inequality for low Reynolds numbers
- problems with variable (nonlinear) viscosity

The incompressible flow problem to be dealt with is the well-known benchmark 'flow around a cylinder' developed in 1995 for the priority research program "Flow simulation on high-performance computers" under the auspices of the DFG, the German Research Association [24]. This project was intended to facilitate the evaluation of various numerical algorithms for the incompressible Navier-Stokes equations in the laminar flow regime. A quantitative comparison of simulation results is possible on the basis of relevant flow characteristics such as drag and lift coefficients, for which sufficiently accurate reference values can be obtained. Moreover, the efficiency of different solution techniques can be analyzed in an objective manner.

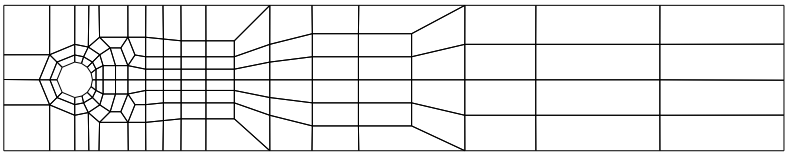

Mesh information			$\tilde{Q}_1/Q_0$
Level	Elements	Vertices	Unknowns
1	156	130	702
2	572	520	2686
3	2184	2080	10608
4	8528	8320	42016
5	33696	33280	167232
6	133952	133120	667264

Table 1. Coarse mesh and geometrical details for the 'flow around a cylinder' configuration for $\tilde{Q}_1/Q_0$ on different levels of mesh refinement

4.1 Stationary flow around a cylinder: $Re = 20$

We consider the steady incompressible flow around a cylinder with circular cross-section which at $Re = 20$ is mainly dominated by diffusion and could be simulated even by the standard Galerkin method without any extra stabilization. However, a certain stabilization is necessary for solving the resulting linear systems with iterative solvers while the central differencing scheme, that means the standard Galerkin approach, usually leads to divergence if using the multigrid solvers. The drag and lift coefficients should approach the reference values $C_D = 5.5795$ and $C_L = 0.01061$ during mesh refinement. The examined stabilization techniques for the convective term have employed the described streamline-diffusion, the FEM upwinding and the edge-stabilization via $j_{2,2}$. Here, we list the number of resulting nonlinear iterations (NL) and the averaged number of multigrid sweeps per nonlinear iteration (AVMG) to gain a prescribed tolerance (here: 1 digit).

gradient formulation								
Stab.	$j_{2,2}$			SD		UPW		Central
	γ			δ^*				
Level	0.0001	0.001	0.01	0.1	0.5	0.1	1.0	
Drag ($C_D = 5.5795$)								
3	5.5874	5.5940	5.6186	5.7144	6.0354	5.6700	6.1152	5.6470
4	5.5855	5.5864	5.5901	5.6417	5.7977	5.6005	5.7460	5.6040
5	5.5813	5.5815	5.5823	5.6020	5.6655	5.5841	5.6197	5.5862
6	5.5800	5.5800	5.5803	5.5868	5.6092	5.5806	5.5882	5.5812
Lift ($C_L = 0.01061$)								
3	0.007328	0.007907	0.008874	0.006933	0.004884	0.005699	-0.002169	0.006237
4	0.009698	0.009806	0.010022	0.008633	0.007506	0.009697	0.007025	0.008604
5	0.010382	0.010398	0.010436	0.009914	0.009227	0.010483	0.010232	0.010043
6	0.010560	0.010562	0.010566	0.010394	0.010065	0.010598	0.010733	0.010471
NL/AVMG								
3	12/3	12/3	12/13	11/3	11/3	10/3	10/3	*/*
4	12/3	12/3	12/11	12/3	11/2	11/3	10/3	*/*
5	12/2	12/2	12/9	12/2	12/2	12/2	11/3	*/*
6	12/2	12/2	12/8	12/2	12/2	12/2	12/2	*/*

Table 2. Drag and lift coefficients for gradient formulation with various stabilization techniques for $Re = 20$

deformation formulation								
Stab.	$j_{2,2}$			SD+j_1		UPW+j_1		central
	γ			$(\delta^* = 0.1)\,\gamma$				
Level	0.0001	0.001	0.01	0.0	0.1	0.0	0.1	
Drag ($C_D = 5.5795$)								
3	5.5913	5.5906	5.6060	5.6764	5.6772	5.5914	5.5921	5.5970
4	5.5846	5.5838	5.5811	5.6261	5.6264	5.5847	5.5850	5.5865
5	5.5810	5.5807	5.5790	5.5974	5.5975	5.5810	5.5811	5.5814
6	5.5799	5.5798	5.5793	5.5856	5.5856	5.5799	5.5799	5.5800
Lift ($C_L = 0.01061$)								
3	0.007993	0.008350	0.009084	0.008197	0.008219	0.007932	0.007964	0.008013
4	0.009893	0.009956	0.010120	0.009402	0.009412	0.009883	0.009894	0.009581
5	0.010432	0.010441	0.010464	0.010170	0.010173	0.010431	0.010434	0.010330
6	0.010572	0.010573	0.010574	0.010465	0.010465	0.010572	0.010573	0.010545
NL/AVMG								
3	12/3	12/3	12/14	12/3	12/3	12/5	12/3	*/*
4	12/3	12/2	12/12	12/2	12/2	12/5	12/2	*/*
5	12/3	12/2	12/8	12/5	12/2	12/11	12/2	*/*
6	12/4	12/2	12/8	12/9	12/2	12/12	12/2	*/*

Table 3. Corresponding drag and lift coefficients for deformation tensor formulation for $Re = 20$

Then, from Table 2 and 3 the following conclusions can be drawn:

- **Streamline-diffusion and upwinding:**
  - The accuracy depends significantly on the user-defined parameter δ^*.
  - The multigrid solver behaves much better, in the case of the deformation tensor formulation, with the additional edge-oriented stabilization j_1 since the influence of the kernel function due to the discrete Korn's inequality has been deleted (see [22]).
- **Edge-oriented stabilization $j_{2,2}$:**
  - The accuracy is much less sensitive w.r.t. the value of the user-defined parameter γ.
  - For both gradient and deformation tensor formulations, the multigrid solver is only slightly sensitive w.r.t. over and under-stabilization.
  - There is no need for the additional edge-oriented stabilization j_1.

The 'classical' stabilization methods may be analyzed in the framework of artificial diffusion methods, and it is immediately clear that the gain of more stabilization is coupled with losses of accuracy if too much diffusion is added (for instance, see [2]). Therefore, a very important factor is the local Re number which measures the ratio between diffusive and convective terms w.r.t. the mesh size, and hence the need of additional diffusion in certain flow directions. In contrast, edge-oriented stabilization can be seen in the framework of strengthening the continuity for the finite element space, so that the adding of the stabilization terms is more related to the structure of the FEM space, rather than to the local Reynolds number. Moreover, another interpretation is that - in contrast to this local Re number approach - the additional stabilization is mainly due to the smoothness of the (discrete) solution such that not the amount of convection, but of smoothness of the solution is the driving force. This could explain why the accuracy achieved for the computation of the drag and lift coefficients is much higher since the solution is quite smooth for this flow configuration.

4.2 Stationary flow around a cylinder: $Re = 1$

One of the reasons why edge-oriented stabilization was becoming so attractive for low order nonconforming finite element methods is its ability to handle flow problems in the range of very small Re numbers, that means more or less Stokes flow, if formulated in terms of the symmetric gradient $\mathbf{D}(\boldsymbol{v})$ of velocity [1, 9, 22]. Therefore, we continue our computational tests to demonstrate the efficiency of the proposed edge-oriented stabilization for this situation. However, in this case we mainly concentrate on the solver aspects, that means the robustness of the multigrid solver w.r.t. Korn's inequality since the accuracy is not the critical case (see [22]) for these flow configurations. Nevertheless, we apply the different stabilization techniques, including upwinding and streamline-diffusion, also for this low Re number problem, hereby formulated in terms of the gradient of velocity, too. In principle, there is no need for any stabilization in this case, but as it becomes clear from Table 4, there is also no negative side effect such that edge-oriented stabilization is a (potential) black box candidate for low and medium Re numbers, despite the fact that there is no local Re number for an explicit control of the amount of involved convection.

gradient formulation							
Stab.	$j_{2,1}$		SD		UPW		Central
	γ		δ^*				
Level	0.001	0.01	0.1	0.5	0.1	1.0	
Drag ($C_D = 3142.4$)							
4	3127.4	3127.4	3127.4	3127.4	3127.4	3127.4	3127.4
5	3138.6	3138.6	3138.6	3138.6	3138.6	3138.6	3138.6
6	3141.5	3141.5	3141.5	3141.5	3141.5	3141.5	3141.5
Lift ($C_L = 30.865$)							
4	30.525	30.525	30.526	30.526	30.525	30.525	30.526
5	30.780	30.780	30.780	30.780	30.780	30.780	30.780
6	30.844	30.844	30.844	30.844	30.844	30.844	30.844
NL/AVMG							
4	3/2	3/2	3/2	3/2	3/2	3/2	3/2
5	4/2	4/2	4/2	4/2	4/2	4/2	4/2
6	4/2	4/2	4/2	4/2	4/2	4/2	4/2

Table 4. Drag and lift coefficients and convergence results for $Re = 1$ for the gradient formulation

Next, we apply the different stabilization techniques for $Re = 1$, but now formulated in terms of the symmetric gradient of the velocity. Table 5 shows that applying edge-oriented stabilization techniques, with the jump of function values (18) in conjunction with upwinding or streamline-diffusion or central differencing, or purely with our proposed jump of the gradient, leads to optimal results.

deformation formulation							
Stab.	$j_{2,1}$		SD+j_1		UPW+j_1		central
	γ		$(\delta^* = 0.1)\,\gamma$				
Level	0.001	0.01	0.0	0.1	0.0	0.1	
Drag ($C_D = 3142.4$)							
4	3132.5	3133.6	3132.4	3133.1	3132.4	3133.1	3132.4
5	3139.9	3139.9	3139.9	3140.1	3139.9	3140.1	3139.9
6	3141.8	3141.6	3141.8	3141.8	3141.8	3141.8	3141.8
Lift ($C_L = 30.8657$)							
4	30.658	30.668	30.658	30.667	30.657	30.666	30.658
5	30.813	30.810	30.813	30.816	30.813	30.816	30.813
6	30.852	30.849	30.853	30.853	30.853	30.853	30.853
NL/AVMG							
4	4/3	4/2	4/29	4/2	4/29	4/2	4/29
5	4/3	4/2	5/98	4/2	4/99	4/2	5/98
6	4/3	4/2	5/154	4/2	5/154	4/2	5/154

Table 5. Drag and lift coefficients and convergence results for $Re = 1$ with the symmetric gradient

Moreover, in order to examine the correct order α in $|E|^\alpha$ (see (19)) for low Re numbers, we perform tests with different values for α and γ with the deformation formulation. Table 6 shows that the multigrid solver for the variant $j_{2,1}$ (behaving like γh) is independent of the refinement in contrast to variant $j_{2,2}$ (behaving like γh^2) which significantly depends on the refinement level due to under-stabilization.

Stab.	$j_{2,2}$			$j_{2,1}$		
γ	0.01	0.1	1.0	0.001	0.01	0.1
Drag ($C_D = 3142.4$)						
4	3132.4	3132.7	3134.9	3132.5	3133.6	3147.7
5	3139.9	3139.9	3140.1	3139.9	3139.9	3142.2
6	3141.8	3141.8	3141.8	3141.8	3141.6	3141.5
Lift ($C_L = 30.8657$)						
4	30.657	30.660	30.687	30.658	30.668	30.908
5	30.813	30.814	30.816	30.813	30.810	30.863
6	30.853	30.853	30.853	30.852	30.849	30.857
NL/AVMG						
4	5/18	4/4	4/3	4/3	4/2	3/6
5	9/20	4/6	4/2	4/3	4/2	3/6
6	11/22	4/10	4/3	4/3	4/2	4/6

γ	0.01	0.05	0.1	0.5	0.01	0.05	0.1	0.5
Level	$j_{2,1}$				$j_{2,2}$			
3	4/2	4/2	4/4	–	4/7	4/3	4/2	4/2
4	4/2	4/2	4/5	–	4/14	4/6	4/4	4/2
5	4/2	4/2	4/5	–	4/19	4/10	4/7	4/3
6	4/2	4/2	4/6	–	4/24	4/16	4/11	4/6

Table 6. Nonlinear iterations (NL)/Averaged multigrid sweeps (AVMG) per nonlinear iteration for $Re = 1$ with deformation tensor formulation and edge-oriented stabilizations $j_{2,1}$ (with order h) and $j_{2,2}$ (with order h^2)

For summarizing these tests for stationary flow configurations with low Re numbers, we finally test our proposed unified stabilization term in (22) with a wide range of 'free' constants γ for both flow around cylinder configurations, that means again for $Re = 1$ and $Re = 20$: Here, we set $\gamma^* = 10\gamma$ (see (22)). Then, Table 7 illustrates for the proposed edge-oriented stabilization that:

- the accuracy is, surprisingly, quite independent of the 'free' parameter γ which means that variations of γ between 0.0001 and 0.01 are easily possible.
- the multigrid solver is also working perfectly up to a 'small' sensitivity w.r.t. over-stabilization, that means for $\gamma \geq 0.01$.

$\sum_{\text{edge E}} \gamma \max(10\nu h_E, h_E^2) \int_E [\nabla \boldsymbol{u}][\nabla \boldsymbol{v}] d\sigma$									
γ	0.0001	0.001	0.01	0.0001	0.001	0.01	0.0001	0.001	0.01
Level	drag			lift			solver		
deformation formulation, $Re = 1$									
4	3132.5	3133.6	3147.7	30.658	30.668	30.908	4/3	4/2	3/6
5	3139.9	3139.9	3142.2	30.813	30.810	30.863	4/3	4/2	3/6
6	3141.8	3141.6	3141.5	30.852	30.849	30.857	4/4	4/2	4/12
gradient formulation, $Re = 1$									
4	3127.5	3128.2	3140.7	30.535	30.613	31.066	4/2	4/2	3/9
5	3138.6	3138.2	3139.2	30.783	30.813	30.966	4/2	4/2	3/9
6	3141.4	3141.0	3140.2	30.846	30.858	30.914	4/2	4/2	3/7
deformation formulation, $Re = 20$									
4	5.5844	5.5815	5.5688	0.009890	0.009934	0.010087	12/2	12/2	12/11
5	5.5809	5.5795	5.5725	0.010430	0.010417	0.010375	12/2	12/2	12/8
6	5.5799	5.5793	5.5759	0.010571	0.010559	0.010501	12/2	12/2	12/8
gradient formulation, $Re = 20$									
4	5.5850	5.5818	5.5651	0.009698	0.009802	0.010075	12/3	12/3	12/11
5	5.5811	5.5797	5.5709	0.010379	0.010376	0.010376	12/2	12/2	12/9
6	5.5799	5.5794	5.5753	0.010558	0.010548	0.010503	12/2	12/2	12/8

Table 7. Drag and lift coefficients and multigrid convergence results with the proposed unified jump term

4.3 Nonstationary flow around a cylinder: $Re = 100$

Next, we analyze the nonstationary case of periodically oscillating flow for a medium Reynolds number, here $Re = 100$ for the 'flow around a cylinder' benchmark [24], with the aim to examine the (spatial) accuracy of the different stabilization techniques. The simulation is performed for $T = [0, 3]$, started with a fully developed solution, for different levels of mesh refinement; here, we perform a fully implicit approach (see [23]) with small time stepping size to minimize the influence of errors coming from the time discretization. Figure 2 shows the time-dependent plots for the lift force values - the most critical quantity in these tests [24] - for different mesh levels and for different stabilization techniques, while Table 8 provides the maximum amplitudes and the Strouhal number (for the frequencies) of the lift value for this periodically oscillating flow.

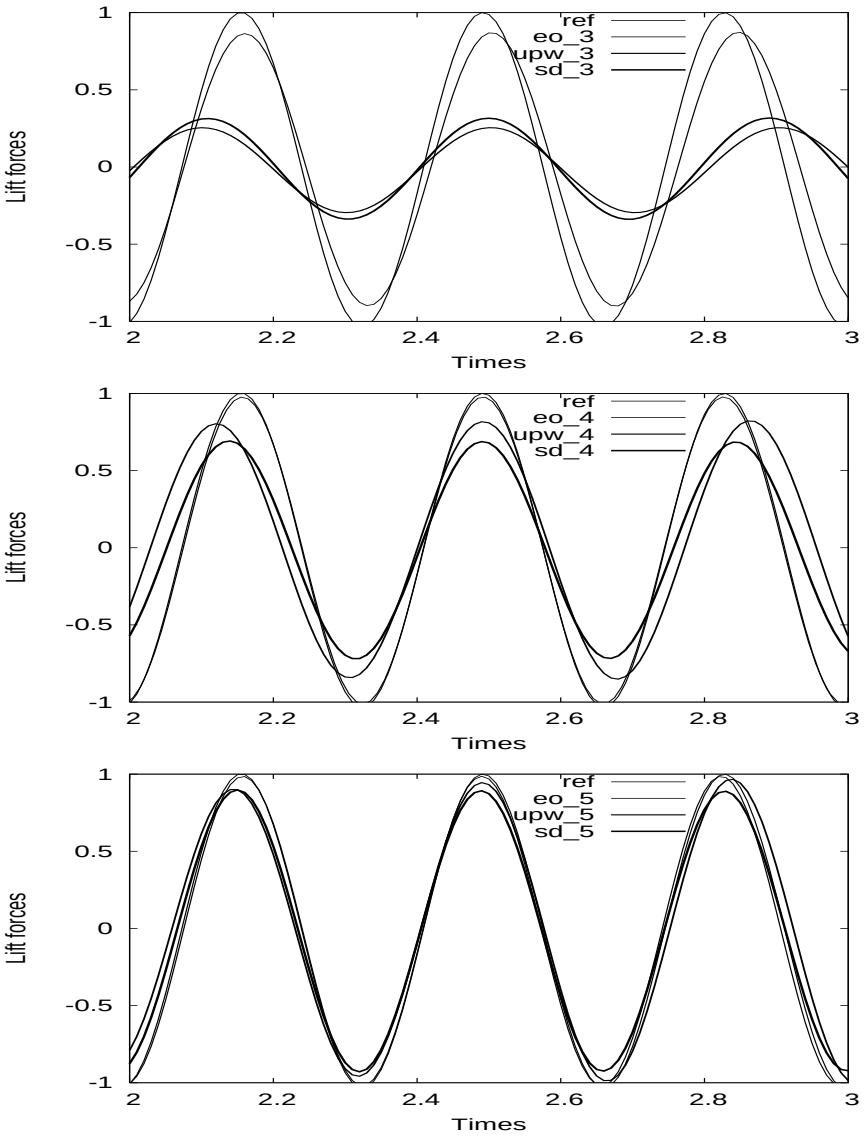

Fig. 2. Reference results for lift vs. results for the different stabilizations (in gradient formulation) for SD-0.1, UPW-0.1 and edge-oriented stabilization EO-0.1

stab.	$j_{2,2}$	SD($\delta^*=0.1$)	UPW ($\delta^*=0.1$)	$j_{2,2}$	SD($\delta^*=0.1$)	UPW ($\delta^*=0.1$)
Level	Maximum amplitude			Strouhal number		
3	0.8750	0.3171	0.2543	0.29126	0.25862	0.23904
4	0.9753	0.6878	0.8214	0.29810	0.26906	0.28436
5	0.9858	0.8864	0.9664	0.30075	0.28708	0.29557
ref	~ 1.0060			~ 0.3020		

Table 8. Maximum amplitude and Strouhal number for the lift value for $Re = 100$

These results clearly show that also in this case of medium Re numbers, which lead to self-induced periodically oscillating flow, the proposed edge-oriented stabilization is significantly more accurate than the applied upwinding, resp., streamline-diffusion variants. Particularly on coarse meshes, the differences w.r.t. the amplitude and especially the frequency ('Strouhal number') of the oscillations are clearly visible and recommend this new approach for fully time-dependent flow configurations in the range of medium Re numbers, too.

4.4 Standing Vortex: $Re = \infty$

To verify the advantageous dissipative properties of the edge-oriented stabilization approach, we consider as next test configuration the well-known 'Standing Vortex' problem [8], in which case the incompressible Navier-Stokes equations for inviscid flow ($Re = \infty$) are solved in a unit square:

$$\frac{\partial \boldsymbol{u}}{\partial t} + \boldsymbol{u} \cdot \nabla \boldsymbol{u} + \nabla p = 0, \quad \nabla \cdot \boldsymbol{u} = 0 \qquad \text{in } \Omega = (0,1) \times (0,1) \tag{26}$$

The initial condition is an axisymmetric vortex which also represents the exact steady-state solution. In polar coordinates, the velocity $\boldsymbol{u}$ can decomposed into the radial component $\boldsymbol{u}_r$ and the angular component $\boldsymbol{u}_\theta$ which are initialized by

$$\boldsymbol{u}_r = 0, \quad \boldsymbol{u}_\theta = \begin{cases} 5r, & r < 0.2, \\ 2 - 5r, & 0.2 \le r \le 0.4, \\ 0, & r > 0.4, \end{cases} \tag{27}$$

where $r = \sqrt{(x-0.5)^2 + (y-0.5)^2}$ denotes the distance from the center. The aim of the following simulations is to check which discretization schemes preserve the original vortex.

The numerical results produced by the different types of stabilization techniques are compared with the exact solution in Fig. 3. They were obtained at $T = 3$ on an equidistant mesh of 64×64, 128×128 and 256×256 quadrilateral elements, respectively, using again a fully implicit time stepping approach (see [23]) with small time steps to eliminate the influence of the temporal discretization errors. Since in this configuration the local Re number is not defined, that means $Re_T = \infty$, the upwinding scheme deteriorates towards the simple first-order, but monotone and oscillation-free upwind method. In the case of the streamline-diffusion scheme, we cancelled the relation to the local Re number. Instead, we multiplied the stabilization term by $\delta_T = \delta^* \cdot h_T$ (compare with (16)), and we only varied the value of δ^* in the following calculations.

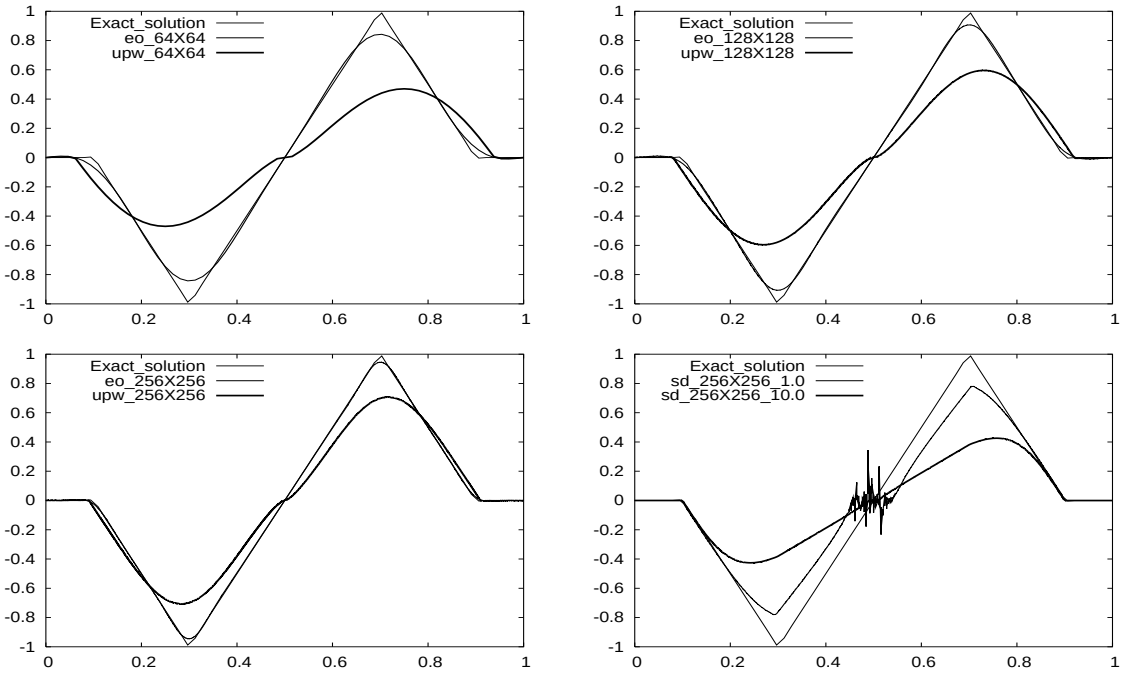

Fig. 3. Cutline of the x-velocity component for the 'Standing Vortex' problem: Comparison of the different stabilization techniques for different mesh levels

The results show the enormous potential of the edge-oriented stabilization for such kind of flow problems. It is obvious that the (first order) upwinding and also the streamline-diffusion method (here: with $\delta^* = 10$) introduce, as expected, too much artificial diffusion (keep in mind that the exact velocity components should have an absolute value of 1). Therefore, one might try to reduce the amount of numerical diffusion of the streamline-diffusion approach by using smaller values for the parameter δ^*. However, in that case, severe spurious numerical oscillations in combination with massive over- and undershooting of the solution arise and render the discrete approximation to be worthless; see the corresponding snapshots in Fig. 4. Moreover, and very surprising for us, massive problems occur in the center of the domain: here, the exact solution is very smooth, but the sign of the velocity components changes. As a result for this configuration in which case the physically correct solution is a so-called *transonic rarefraction* solution [16], the discrete approximation leads to *entropy violating shocks* and requires special techniques for an entropy fix. This problem can be clearly seen in Fig. 3, where at the center ($x = y = 0.5$) the solutions for the upwinding, resp., streamline-diffusion approaches cannot reproduce the linear shape. In contrast, the edge-oriented approach does not show any problem in this case which is very amazing and requires more numerical studies which will be part of a forthcoming paper.

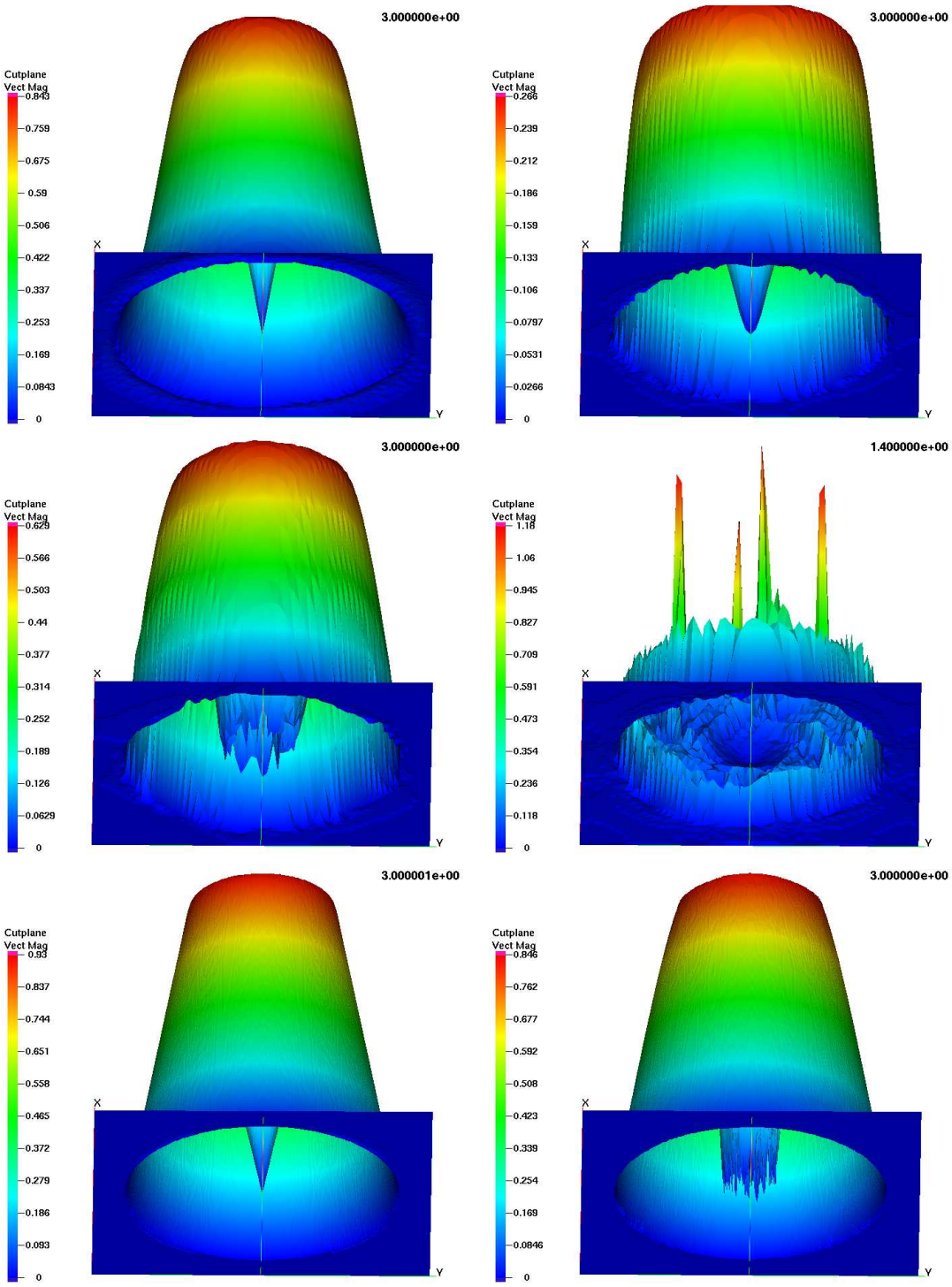

Fig. 4. 3D presentation of the norm of the velocity (VECT MAG) for the 'Standing Vortex' problem: edge-oriented vs. streamline-diffusion ($\delta^* = 10$) for $h = 1/64$ (TOP); streamline-diffusion with $\delta^* = 0.5$ and $\delta^* = 0$ (= central differencing) for $h = 1/64$ (MIDDLE); edge-oriented vs. streamline-diffusion ($\delta^* = 0.5$) for $h = 1/256$ (BOTTOM)

4.5 Non-newtonian case: Shear-dependent viscosity

In the next simulations, we consider the case of non-newtonian flow in which case we employ the standard *Power Law* model for the viscosity function ν. However, in this case, we are confronted with the question of how to choose a value for ν, and also for $\mathbf{D}(\boldsymbol{u}_h)$ due to $\nu = \nu(D_{II}(\boldsymbol{u}))$ on the edges of the mesh cells which is required in the edge-oriented stabilization approach (keep in mind that $\mathbf{D}(\boldsymbol{u}_h)$ is not defined on edges due to the nonconformity such that an appropriate postprocessing has to be applied). In the following, we prescribe $\nu(D_{II}(\boldsymbol{u})) = \nu_0(\epsilon + D_{II}(\boldsymbol{u}))^\alpha$ which leads to 'shear-thickening' ($\alpha \geq 0$) or 'shear-thinning' ($\alpha \leq 0$). For the special parameter choices $\epsilon = 10^{-1}, \nu_0 = 1$ and $|\alpha| = 0.35$, the viscosity function ν varies locally by a factor of 10 ($\alpha = 0.35$) or even 30 ($\alpha = -0.35$). Figure 5 shows corresponding plots of the resulting viscosity function $\nu(D_{II}(\boldsymbol{u}))$ for the converged solution $\boldsymbol{u}$ of these nonlinear problems.

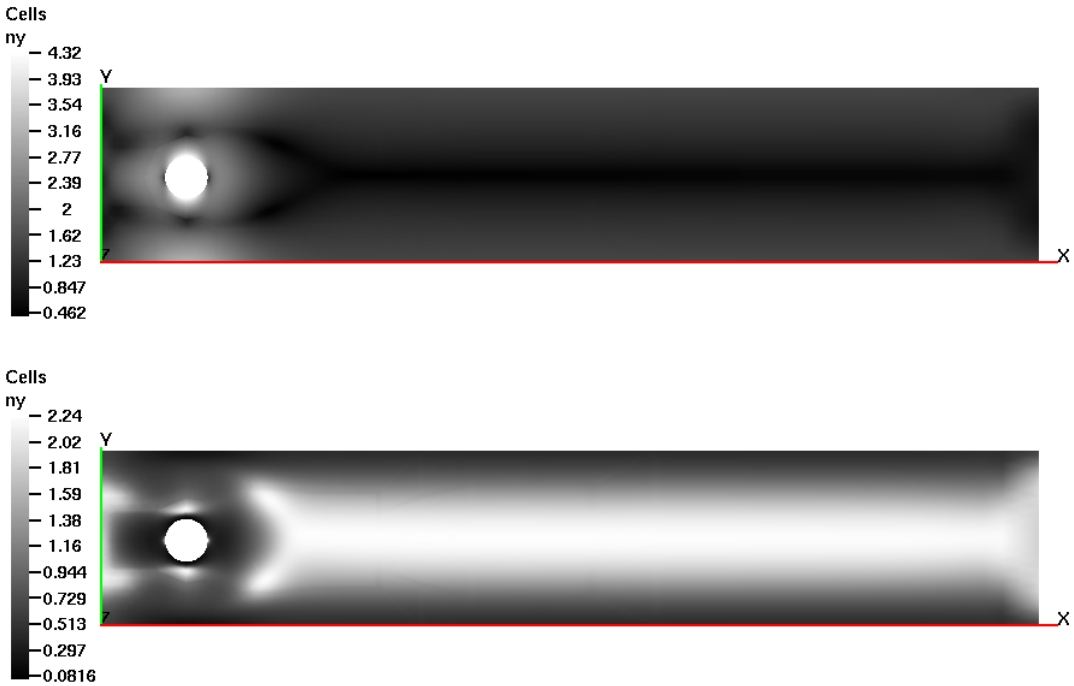

Fig. 5. The resulting viscosity for the described cases of shear thickening/thinning

Looking at this locally changing behaviour of the viscosity function, the question arises of how to choose the stabilization parameters $\gamma \cdot \nu$ in (22) on each edge. In the following Table 9 we show results for the version ν_{const} in which case ν was fixed to be the minimum value of the (global) viscosity. In contrast, the approach ν_{local} is based on the local size of the viscosity ν on every edge and takes into account the local variations due to changes w.r.t. the value of $D_{II}(\boldsymbol{u})$. As expected, the locally adapted choice ν_{local} shows a better nonlinear convergence behaviour (number of nonlinear iterations NL), and the corresponding linear multigrid behaviour (averaged number of multigrid sweeps per nonlinear cycle AVMG) is significantly better, due to a possible underestimation of the value ν_{const} in the stabilization procedure; the case of no stabilization at all shows the expected problems due to the failure of Korn's inequality.

Additionally, we discuss the aspect of selecting the appropriate stabilization parameter γ in $\gamma \cdot \nu_{const}$, resp., $\gamma \cdot \nu_{local}$. The results in Table 9 demonstrate again the improved behaviour of the locally adaptive stabilization parameter ν_{local}, and that γ can be chosen from a quite wide range.

	$\alpha = -0.35$			$\alpha = 0.35$		
Level	no stab	ν_{const}	ν_{local}	no stab	ν_{const}	ν_{local}
3	26/48	24/4	24/3	17/7	17/6	17/5
4	26/140	25/5	25/3	18/15	17/8	17/5
5	27/414	24/6	24/3	50/212	17/10	17/5
6	–	24/7	24/3	–	17/12	17/5
Level 4						
γ	0.1	0.01	0.001	0.1	0.01	0.001
$\gamma \cdot \nu_{const}$	25/4	25/11	25/15	17/6	17/14	17/27
$\gamma \cdot \nu_{local}$	25/3	25/3	25/8	17/5	17/10	17/23

Table 9. NL/AVMG for different choices of stabilization ($\epsilon = 10^{-1}, \nu_0 = 1$) for $\nu = \nu_0(\epsilon + D_{II}(\boldsymbol{u}))^{\alpha}$

4.6 Non-newtonian case: Pressure and shear-dependent viscosity

Finally, we consider again the case of low *Re* numbers while the viscosity now has the form:

$$\nu(p, D_{II}(\boldsymbol{u})) = (\epsilon + \frac{1}{\sqrt{\epsilon + \exp(\beta\, p)}} + D_{II}(\boldsymbol{u}))^{\frac{r}{2}-1} \tag{28}$$

Then, the results in Table 10 essentially confirm our previous results, namely that the local evaluation ν_{local} of the (nonlinear) viscosity leads to improved results regarding the nonlinear and particularly the linear solution behaviour, and that the 'free' parameter γ does not have a significant influence onto the convergence rates for a wide range of values.

γ	0.0	0.0001	0.001	0.01	0.0001	0.001	0.01
Level	no stab	ν_{local}			ν_{const}		
r=3.0							
3	7/6	7/2	7/2	6/2	6/2	6/2	5/2
4	7/19	6/2	6/2	6/2	7/2	6/2	6/3
5	7/51	7/2	6/2	6/2	7/3	7/2	6/3
6	9/108	7/2	7/2	6/2	10/1	7/2	5/3
r=1.5							
3	7/7	6/2	7/2	7/2	6/2	6/2	5/2
4	8/22	7/2	7/2	7/2	7/2	6/2	6/3
5	9/61	7/2	7/2	6/2	7/2	7/2	6/3
6	14/65	11/1	9/1	6/2	10/1	7/2	5/3
r=1.1							
3	12/6	14/2	15/2	11/2	11/2	9/2	7/3
4	16/11	17/2	15/2	12/2	13/2	9/2	7/4
5	20/23	18/2	15/2	13/3	14/2	10/4	8/6
6	24/44	19/2	14/2	12/3	15/2	11/3	10/7

Table 10. NL/AVMG for pressure and shear-dependent viscosity

5 Conclusions and outlook

Egde-oriented stabilization approaches including jump terms of the gradient on the edges of the computational mesh together with low order nonconforming FEM spaces have been numerically analyzed for incompressible flow problems. The computational tests considered cases of various Re numbers (ranging from $Re = 1$, resp., Stokes flow, over medium Re numbers with periodically oscillating flow phenomena up to the case '$Re = \infty$'). Moreover, formulations including the gradient as well as the symmetric deformation tensor ('Korn's inequality') of the velocity have been considered, and we examined non-newtonian problems with pressure and shear-dependent viscosity. The proposed edge-oriented stabilization term involves only the gradient of discrete test and trial functions (leading to reduced assembling costs), which together with a special parameter setting taking into account the local size of the viscosity, if available, requires only one 'free' parameter γ. The numerical tests for various prototypical problems settings have shown that, in contrast to classical stabilization schemes of upwinding or streamline-diffusion type, the influence of this parameter onto the resulting accuracy, robustness and efficiency is surprisingly small.

Summarizing these computational tests, we have shown that with these special edge-oriented FEM stabilization methods:

- we can stabilize the lack of coercivity ('Korns's inequality') for problems formulated in terms of the symmetric part of the velocity gradient.
- we can handle problems for most relevant Re numbers, even in the limit of inviscid flow.
- we can successfully realize strategies for simulating non-newtonian flow with pressure and shear-dependent viscosity.
- we can solve the resulting linear generalized Oseen problems in conjunction with standard multigrid components which preserve the original FEM data structure.

Based on these positive results for a wide range of typical flow simulations, we can state that the proposed stabilisation technique may be an interesting candidate for black-box components in CFD codes. Therefore, one future aim is to study the corresponding numerical behaviour w.r.t. accuracy and robustness in cases of turbulence effects, visco-elastic fluids and multiphase flow settings including pure transport problems which are coupled with the Navier-Stokes equations. Moreover, we are recently examining improved iterative solvers which explicitely employ the complete stiffness matrix, based on the extended matrix structures due to the additional coupling of FEM basis functions by the edge-oriented jump terms.

Looking more carefully at the resulting matrix stencils for the terms $\int_E [\nabla\phi_i][\nabla\phi_j] d\sigma$, the matrix structure can be seen in Fig. 6. While the matrix stencils are always increased, leading to couplings between FEM basis functions which do not have common local support, it is also visible that reduced integration may lead to a different amount of additional memory requirements. Recently, we have been successful to extend our CFD package FEATFLOW such that the complete stabilization matrix is stored and, hence, corresponding Linear Algebra components (SOR methods, ILU(k) smoothers, SPAI schemes) can be directly applied which results in much better CPU timings and an improved convergence behaviour. These computational studies, also in work for conforming linear and quadratic finite elements, and together with numerical tests regarding the accuracy and robustness of the reduced matrix stencil in Fig. 6 will be part of a forthcoming paper.

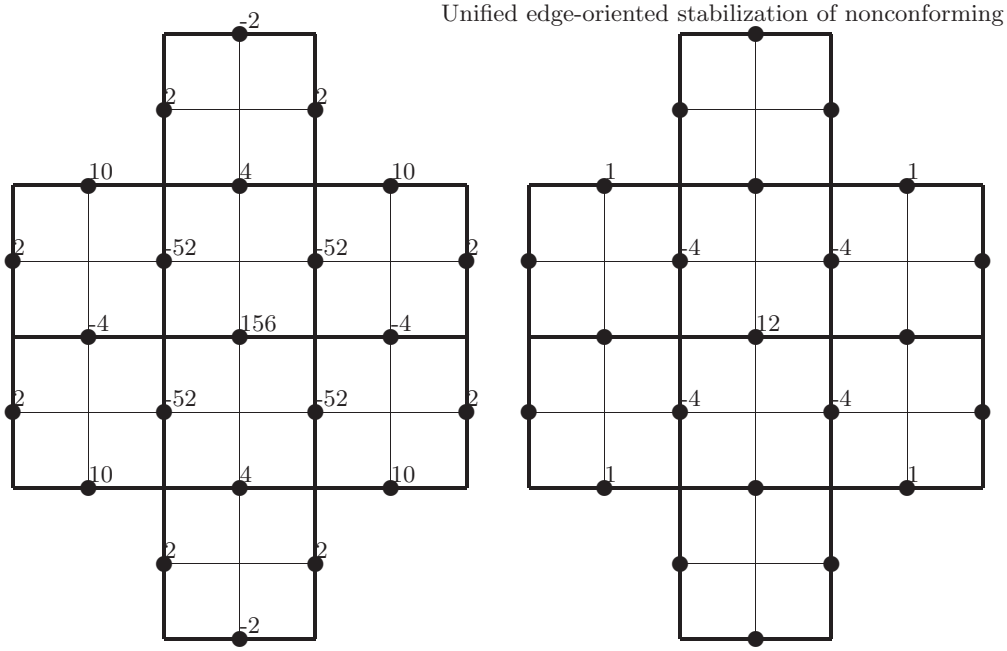

Fig. 6. Stencil for $\int_E [\nabla\phi_i][\nabla\phi_j]d\sigma$ with exact (left) and with 1-point Gauss quadrature (right)

References

[1] Brenner, S. Korn's inequalities for piecewise H^1 vector fields. *Math. Comp.*, 73:1067–1087, 2004.

[2] Brezzi, F., Franca, L. P., Hughes, T.J.R., and Russo A. Stabilization techniques and subgrid scales capturing. In *The state of the Art in Numerical Analysis*, IAM Conference Series **63**, pages 391–406. Oxford Univ. Press, 2001. I.S. Duff and G.A. Waston Eds. 1996.

[3] Burman, E. A unified analysis for conforming and nonconforming stabilized finite element methods using interior penalty. *SINUM*, 2004. to appear.

[4] Burman, E. and Hansbo, P. Stabilized Crouzeix-Raviart element for the Darcy-Stokes problem. Technical report, Chalmers Finite Element Center, 2003. Preprint 2003-15.

[5] Burman, E. and Hansbo, P. A stabilized non-conforming finite element method for incompressible flow. *Comp. Meth. Mech. Eng.*, 2003. to appear, Preprint 2004-6, Chalmers Finite Element Center.

[6] Burman, E. and Hansbo, P. Edge stabilization for galerkin approximations of convection-diffusion-reaction problems. *Comp. Meth. Mech. Eng.*, 193:1437–1453, 2004.

[7] Burman, E. and Fernández, M. and Hansbo, P., editor. *Edge stabilization: an interior penalty method for the incompressible Navier-Stokes equation*, volume I, 2004. ECCOMAS 4.

[8] Gresho, P.M. and Chan, S.T. On the theory of semi-implicit projection methods for viscous incompressible flow and its implementation via a finite element method that also introduces a nearly consistent mass matrix. II: Implementation. *Int. J. Numer. Methods Fluids*, 11(5):621–659, 1990.

[9] Hansbo, P. and Larson, M. G. A simple nonconforming bilinear element for the elasticity problem. Preprint 2001-01, Chalmers Finite Element Center, Chalmers University of Technology, Göteborg Sweden, 2001. h1750-P.

[10] Hron, J., Malék, J., Necãs J., and Rajagopal, K. R. Numerical simulations and global existence of solutions of two-dimensional flows of fluids with pressure- and shear-dependent viscosities. *Mathematics and Computers in Simulation*, 61:297–315, 2003.

[11] Hughes, T. J. R. and Brooks, A.N. A multidimensional upwind scheme with no crosswind diffusion. In *Finite element methods for convection dominated flows*, 1979. New York: ASME 1979.

[12] John, V., Maubach, J. M., and Tobiska, L. Nonconforming streamline-diffusion-finite-element-method for convection-diffusion problems. *Numer. Math.*, 78:165–188, 1997.
[13] Johnson, C. *Numerical solution of partial differential equations by the finite element method*. Cambridge University Press, 1987.
[14] Knobloch, P. On korn's inequality for nonconforming finite elements. *Technische Mechanik*, 20:205–214, 2000.
[15] Kuzmin, D., Löhner, R., and Turek, S. *Flux-Corrected Transport: Principles, Algorithms, and Applications*. Springer, 2005. Series: Scientific Computing.
[16] Leveque, R.J. *Finite Volume Methods for Hyperbolic Problems*. Cambridge University Press, 2002.
[17] Malék, J., Necãs, J., and Rajagopal, K. R. Global existence of solutions for flows of fluids with pressure and shear dependent viscosities. *Applied Mathematics Letters*, 15:961–967, 2002.
[18] Ouazzi, A., Turek, S., and Hron, J. Finite element methods for the dimulation of incompressible powder flow. *CNME*, :, 2005. to appear.
[19] Rannacher, R. and Turek, S. A simple nonconforming quadrilateral stokes element. *Numer. Methods Partial Differential Equations*, 8:97–111, 1992.
[20] Schaeffer, D.G. Instability in the evolution equation describing incompressible granular flow. *J. of Differential Equations*, 66:19–50, 1987.
[21] Turek, S. *Efficient solvers for incompressible flow problems: An algorithmic and computational approach*. Springer, 1999.
[22] Turek, S., Ouazzi, A., and Schmachtel, R. Multigrid methods for stabilized nonconforming finite elements for incompressible flow involving the deformation tensor formulation. *J. Numer. Math.*, 10:235–248, 2002.
[23] Turek, S., Rivkind, L., Hron, J., and Glowinski, R. Numerical analysis of a new time-stepping θ-scheme for incompressible flow simulations. Technical report, Universität Dortmund, 2005. .
[24] Turek, S. and Schäfer, M. Benchmark computations of laminar flow around cylinder. In E.H. Hirschel, editor, *Flow Simulation with High-Performance Computers II*, volume 52 of *Notes on Numerical Fluid Mechanics*, pages 547–566. Vieweg, 1996. co. F. Durst, E. Krause, R. Rannacher.
[25] Vanka, S.P. Implicit multigrid solutions of Navier-Stokes equations in primitive variables. *J. of Comp. Phys.*, 65:138–158, 1985.